RSC Advances

ROYAL SOCIETY OF CHEMISTRY

www.rsc.org/advances

Journal Name

ARTICLE

Synthesis and characterization of $LiNi_{0.48}Co_{0.18}Mn_{0.3}Mg_{0.02}Ti_{0.02}O_2$ as cathode material for lithium ion battery

Received 00th January 20xx,
Accepted 00th January 20xx

DOI: 10.1039/x0xx00000x

www.rsc.org/

Yan Mo, De Li, Yong Chen,* Bokai Cao, Bo Hou, Zhuo Zhu, and Jianlin Li

The layered oxide material $LiNi_{0.48}Co_{0.18}Mn_{0.3}Mg_{0.02}Ti_{0.02}O_2$ has been synthesized via a co-precipitation assisted solid-phase method, and its crystal structure, morphology and electrochemical properties have been systematically investigated. Rietveld refinement of its X-ray diffraction data indicates a higher degree of the well-ordered crystallographic form, which provides $LiNi_{0.48}Co_{0.18}Mn_{0.3}Mg_{0.02}Ti_{0.02}O_2$ with superior cycle performance and rate capability. The initial discharge capacities of the electrode are 151.5 mAh g^{-1}, 140.1 mAh g^{-1}, 137.1 mAh g^{-1}, 125.2 mAh g^{-1} and 115.3 mAh g^{-1} at the current of 0.5C, 1C, 2C, 3C and 5C, respectively. After 100 cycles at the same rates, 94%, 96%, 96%, 94% and 93% of the initial discharge capacity are retained. The improved electrochemical properties are attributed to the decrease in particle size and suppression of cation mixing due to doping with Mg and Ti. The results of this work indicate that $LiNi_{0.48}Co_{0.18}Mn_{0.3}Mg_{0.02}Ti_{0.02}O_2$ is a promising cathode material for Li-ion batteries.

1. Introduction

Enormous demand for storage of cleanly-generated energy has propelled the development of lithium-ion batteries (LIBs).[1-3] $LiCoO_2$, having an ideal layered structure, has been widely used as the commercial cathode material in LIBs with high operating voltage and good electrochemical performances. However, only half of the reversible capacity of $LiCoO_2$ can be delivered because of its structural degradation caused by the dislocation of lattice oxygen. Additionally, some drawbacks such as low content in the crust, high cost and toxicity of Cobalt hinder its further applications.[4, 5] In recent years, the development of alternative cathode materials with better specific energy density for next-generation LIBs has attracted increasing attention from researchers. The layered multi-component cathode material, $LiNi_{1-x-y}Co_xMn_yO_2$ (NCM), particularly the $LiNi_{0.5}Co_{0.2}Mn_{0.3}O_2$ (NCM523), is one of the most promising candidates. NCM523 is able to increase the performance of the battery with higher reversible capacity, better cycle ability, lower Co^{2+} content and enhanced thermodynamic stability compared with $LiCoO_2$.[6-10] However, it was observed that the unavoidable Li/Ni site-exchange in these materials gives rise to decreased rate capability, structural deformation, and more difficulty in preparation of the pure phase[10-14]. Moreover, other problems such as highly reactive Ni^{4+}, poor stability of conventional electrolyte above 4.2 V versus Li/Li^+, as well as anodic instability and surface side reactions of $LiNi_{0.5}Co_{0.2}Mn_{0.3}O_2$ contribute to its unsatisfactory initial columbic efficiency and capacity fade during cycling[15-17].

One effective method to overcome these issues is to introduce cations such as Mg^{2+},[18] Al^{3+},[19] Cr^{3+},[20] Ti^{4+},[21] Zr^{4+}[22] and V^{5+}[23] as dopants into the layered host structure, which could prevent migration of Ni^{2+} toward Li^+ layer, increase the metal–oxygen bonding energy and increase the number of stable elements in the electrode material. Kang et al. have reported partial substitution of Ni and Mn by Co in layered $Li[Ni_{0.5-x}Mn_{0.5-x}M_{2x}]O_2$ (x = 0, 0.025) enhanced the discharge capacity, cycling stability as well as the thermal stability.[24] Yuan et al. have investigated that doping of Mo in layered $Li[Ni_{(1-x)/3}Mn_{(1-x)/3}Co_{(1-x)/3}Mo_x]O_2$ affected the structure and lead an improved electrochemical performance.[25] It can be seen that binary or ternary doping show potential in improving electrochemical properties of layered oxide cathode materials. However, the effects of multi-elements doping on the electrochemical performances of NCM523 are still unclear, so we try to illustrate it in this paper.

Herein, we have studied the effects of Mg^{2+} and Ti^{4+} co-doping on NCM materials. Mg^{2+} and Ti^{4+} are chosen as the doping elements in $LiNi_{0.5-x}Co_{0.2-x}Mn_{0.3}M^1{}_xM^2{}_xO_2$ to form modified $LiNi_{0.48}Co_{0.18}Mn_{0.3}Mg_{0.02}Ti_{0.02}O_2$. Xu al. proposed that the doping of Mg^{2+}, whose ionic radius size is much larger than Ni^{2+}, Co^{3+} and Mn^{4+}, increased the lattice parameters, significantly facilitated the lithium-ion diffusion and improved rate capability in $Li[Li_{0.2}Ni_{0.13}Co_{0.13}Mn_{0.54}]O_2$ system.[18] Markus also investigated the Ti doping effect in the $Li_1(Ni_xMn_xCo_{1-2x-y}Ti_y)O_2$ system. It was found that such aliovalent doping can improve the energy densities of LIBs, and the stronger oxygen binding of Ti-O can enhance phase stability during cycling.[21] It was excepted that a partial doping with Mg and Ti would have positive effect on the cycling stability as well as the rate capability. The structural changes,

atory of Tropic Biological Resources, MOE; Key Laboratory of Ministry of Education for Advanced Materials in Tropical Island Resources; Hainan Provincial Key Laboratory of Research on Utilization of Si-Zr-Ti Resources; Hainan University, 58 Renmin Road, Haikou 570228, China. E-mail: ychen2002@163.com; Fax: +86- 898-66291383; Tel: +86-898-66279122

surface morphology and electrochemical behavior of the doped NCM materials were studied. We demonstrate that a careful optimization of the doping strategy allows us to achieve a superior electrochemical performance compared to the pristine sample. With the added benefit of reduced Co content, this strategy is a promising route for the low-cost and large-scale production of cathode materials for high performance LIBs.

2. Experimental

2.1 Synthesis of $LiNi_{0.48}Co_{0.18}Mn_{0.3}$ $Mg_{0.02}Ti_{0.02}O_2$

$LiNi_{0.48}Co_{0.18}Mn_{0.3}Mg_{0.02}Ti_{0.02}O_2$ sample was prepared by a co-precipitation method followed by heating at a high temperature. First, the mixed sulfate solution containing $NiSO_4{\cdot}6H_2O$, $CoSO_4{\cdot}7H_2O$, and $MnSO_4{\cdot}H_2O$ (cation molar ratio of 0.48: 0.18: 0.3) with a concentration of 2 mol dm^{-3} was slowly pumped into the reactor at 50 °C under the N_2 atmosphere. Then, the aqueous solutions of $NH_3{\cdot}H_2O$ (as complexing agent) and 4 mol·dm^{-3} NaOH (as precipitator) were also added into the solution at a constant rate to adjust the pH value at 11.0, with vigorous stirring at around 800 rpm for 12 h in the reactor. Then the co-precipitated precursor was filtered and washed with deionized water to remove the residual ions (Na^+, SO_4^{2-}, NH^{4+} or others). It was then dried at 60 °C for overnight. The obtained powder was mixed with 5% excess of Li_2CO_3 and then thoroughly ground together with TiO_2 and MgO by mechanical milling. The mixture was first preheated at 550 °C for 6 h and then calcined at 900 °C for 12 h. For comparison purposes, pure $LiNi_{0.5}Mn_{0.2}Co_{0.3}O_2$ was prepared under the same conditions without adding TiO_2 and MgO.

2.2 Characterization Methods

The crystalline phase structure and phase purity of the as-prepared powder samples were examined by X-ray diffraction (XRD, Panalytical X'pert PRO) with Cu Ka radiation (l = 1.5406 Å) source. XRD data were gathered for 2θ varying between 10° and 80°. Field emission scanning electron microscope (FESEM, Hitachi S-4800) coupled with an energy dispersive X-ray detector (EDX) was used to observe the morphology of the material. The microstructure of the material was analyzed using transmission electron microscope (Tecnai G2 F30, S-TWIN) which was operated at 200 kV. Chemical compositions of samples were determined by an inductively coupled plasmas spectrometer (ICP, Optima 7300 DV).

2.3 Electrochemical Measurement

The positive electrodes were prepared by mixing the as-prepared cathode materials, Ketjen Black and polyvinylidene fluoride (PVDF) in the weight ratio of 8:1:1, and using an appropriate amount of N-methyl-2-pyrrolidine (NMP) as the solvent. After milling thoroughly, homogeneous slurry was obtained. The obtained slurry was coated onto an Al foil and dried overnight under vacuum at 110 °C. The typical loadings of active material in the cathode are 2.5-3.5 mg cm^{-2}. The coin cells were fabricated in an argon-filled glove box by using Lithium as the counter electrode, Celgard 2320 microporous film as the separator, and 1 M $LiPF_6$ in ethylene carbonate (EC) as the electrolyte. The electrochemical properties of the composite electrodes were measured via galvanostatic charge-discharge test using a LAND CT2001A Battery Test System over a potential range of 2.8-4.3V. The cyclic voltammetry (CV) and electrochemical impedance spectroscopy (EIS) measurements were performed on a Biological electrochemical workstation (bio-logic VSP-300). The CV was carried out between 2.7 and 4.4 V at a scan rate of 0.1 mV s^{-1}. The EIS measurements were carried out at a fully charged state in the frequency range from 100 kHz to 0.1 Hz with an amplitude voltage of 5 mV.

3. Results and discussion

3.1 Structural Characterization

Fig. 1a shows the XRD patterns of the $LiNi_{0.5}Co_{0.2}Mn_{0.3}O_2$ and $LiNi_{0.48}Co_{0.18}Mn_{0.3}$ $Mg_{0.02}Ti_{0.02}O_2$ samples. The XRD patterns of all samples can be indexed to a hexagonal α-$NaFeO_2$ structure with the space group of $R\bar{3}m$ [26]. A clear splitting of the (0 0 6 and 1 0 2) and (1 0 8 and 1 1 0) couples of the $LiNi_{0.48}Co_{0.18}Mn_{0.3}$ $Mg_{0.02}Ti_{0.02}O_2$ sample are shown in Fig. 1a, suggesting that the bulk structure is slightly affected by partial Mg and Ti substitution and that a layer structure is well developed. The ratio of the peak intensities of I_{003} and I_{104} is a measure of the degree of cation mixing; the larger the value of I_{003}/I_{104}, the lesser the cation mixing[27]. It can be seen from Table 1, the I_{003}/I_{104} ratio of $LiNi_{0.48}Co_{0.18}Mn_{0.3}Mg_{0.02}Ti_{0.02}O_2$ is

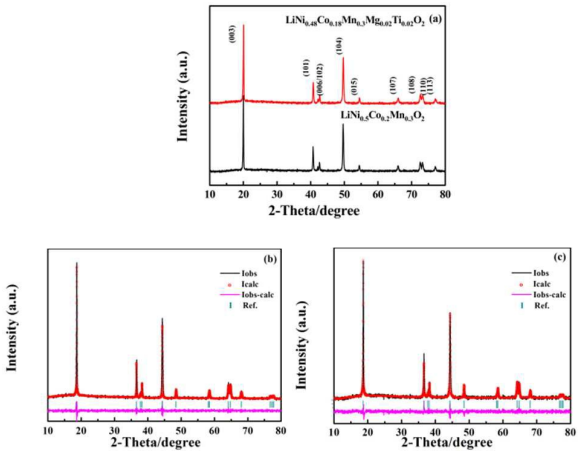

Fig. 1 XRD patterns (a) and Rietveld refinement results (b, c) of $LiNi_{0.5}Co_{0.2}Mn_{0.3}O_2$ and $LiNi_{0.48}Co_{0.18}Mn_{0.3}$ $Mg_{0.02}Ti_{0.02}O_2$.

Table 1. Lattice parameters of the $LiNi_{0.5}Co_{0.2}Mn_{0.3}O_2$ and $LiNi_{0.48}Co_{0.18}Mn_{0.3}$ $Mg_{0.02}Ti_{0.02}O_2$ sample.

Sample	a (Å)	c(Å)	V (Å^3)	$I_{(003)}/I_{(104)}$
$LiNi_{0.5}Co_{0.2}Mn_{0.3}O_2$	2.8790(7)	14.2509(0)	100.72	1.59
$LiNi_{0.48}Co_{0.18}Mn_{0.3}$-$Mg_{0.02}Ti_{0.02}O_2$	2.8829(6)	14.2739(1)	102.83	1.66

Table 2. Structural parameters obtained from Rietveld refinement of the XRD data for the $LiNi_{0.5}Co_{0.2}Mn_{0.3}O_2$ and $LiNi_{0.48}Co_{0.18}Mn_{0.3}Mg_{0.02}Ti_{0.02}O_2$ sample.

	Atom	Li	Ni	M	O	R_{wp}
	Site	3a	3a	3b	3c	(%)
Occ	$LiNi_{0.5}Co_{0.2}Mn_{0.3}O_2$	0.9557	0.0432	0.9568	2.0	10.03
	$LiNi_{0.48}Co_{0.18}Mn_{0.3}Mg_{0.02}Ti_{0.02}O_2$	0.9718	0.0278	0.9722	2.0	10.87

higher than the pristine sample. Preferred orientation effects may also have an effect on relative peak intensities but Rietveld refinements (Fig. 1b-c) of the patterns confirm that the cation mixing is decreased after Mg and Ti doping.

Rietveld refinements were performed for XRD patterns of the pristine and $LiNi_{0.48}Co_{0.18}Mn_{0.3}Mg_{0.02}Ti_{0.02}O_2$ samples by supposing the space group of $R\bar{3}m$. For refinements, Li ions are located in the 3*a* sites, metal ions (M = Ni, Co, Mn, Mg, Ti) occupy the 3*b* site, and oxygen atoms occupy the 6*c* site. The Rietveld results of the lattice parameters and Structural parameters of the pristine and $LiNi_{0.48}Co_{0.18}Mn_{0.3}$ $Mg_{0.02}Ti_{0.02}O_2$ sample are given in Table 1 and Table 2, respectively. The unit cell volume *v*, as well as the parameters *a* and *c* increase with partial Mg and Ti substitution, which can enhance the migration velocity of Li^+ in the bulk phase. This can be ascribed to the fact that the radius of Mg^{2+} (r = 0.72 *Å*) and Ti^{4+} (r = 0.68 *Å*) is larger than that of Ni^{2+} (r = 0.69 *Å*) and Co^{3+} (r = 0.545 *Å*), respectively. Furthermore, it can be seen from Table 2, the reliability factor (R_{wp}) is good and $LiNi_{0.48}Co_{0.18}Mn_{0.3}Mg_{0.02}Ti_{0.02}O_2$ possesses lower values of cation disorder (Ni in Li layer just 2.78%), which agrees well with the results of the intensity ratios of the I_{003}/I_{104}. As mentioned above, it could be concluded that $LiNi_{0.5}Co_{0.2}Mn_{0.3}O_2$ has improved electrochemical performance following the addition of Ti and Mg[28].

3.2 Morphological Characterization

SEM images of the pristine and $LiNi_{0.48}Co_{0.18}Mn_{0.3}Mg_{0.02}Ti_{0.02}O_2$ samples are shown in Fig. 2. It can be observed from Fig. 2a that $LiNi_{0.5}Co_{0.2}Mn_{0.3}O_2$ is composed of near-spherical secondary particles with an average size of about 15 µm. The near-spherical particles consist of irregularly shaped bricks with a lateral dimension of about 400 nm. As shown in Fig. 2b, the primary particle size of $LiNi_{0.48}Co_{0.18}Mn_{0.3}Mg_{0.02}Ti_{0.02}O_2$ sample becomes smaller, which indicates that Mg^{2+} and Ti^{4+} co-doping reduces the particle size of sample, shortens the distance of Li^+ diffusion and improves the electrochemical performance of the sample. From the EDS results (Fig. 3), it is clearly seen that the elements (Ni, Co, Mn, Mg, and Ti) are uniformly distributed in $LiNi_{0.48}Co_{0.18}Mn_{0.3}Mg_{0.02}Ti_{0.02}O_2$. A more reliable analysis of chemical compositions of $LiNi_{0.5}Co_{0.2}Mn_{0.3}O_2$ and $LiNi_{0.48}Co_{0.18}Mn_{0.3}Mg_{0.02}Ti_{0.02}O_2$ sample were done by ICP experiments (Table 3). According to the results in Table 3, the observed molar ratio of Ni, Co and Mn elements in molar ratio for $LiNi_{0.5}Co_{0.2}Mn_{0.3}O_2$ is 0.499: 0.198: 0.303, and Ni, Co, Mn, Mg and Ti elements in molar ratio for $LiNi_{0.48}Co_{0.18}Mn_{0.3}Mg_{0.02}Ti_{0.02}O_2$ sample is 0.478: 0.179: 0.304: 0.019: 0.020, close to the aimed molar ratio. The microstructure of $LiNi_{0.48}Co_{0.18}Mn_{0.3}Mg_{0.02}Ti_{0.02}O_2$ sample was

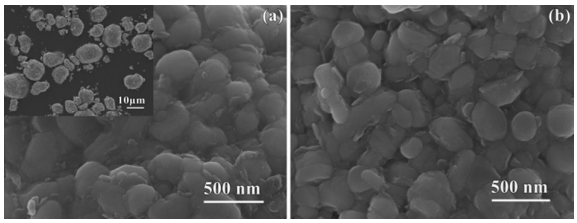

Fig. 2 SEM images of $LiNi_{0.5}Co_{0.2}Mn_{0.3}O_2$ (a) and $LiNi_{0.48}Co_{0.18}Mn_{0.3}Mg_{0.02}Ti_{0.02}O_2$ (b).

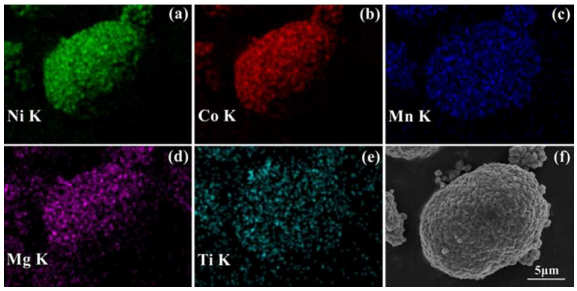

Fig. 3 EDX mapping of the $LiNi_{0.48}Co_{0.2}Mn_{0.3}Mg_{0.02}Ti_{0.02}O_2$ sample: Ni (a), Co (b), Mn (c), Mg (d), Ti (e), and all the five (Ni, Co, Mn, Mg, and Ti) elements together (f).

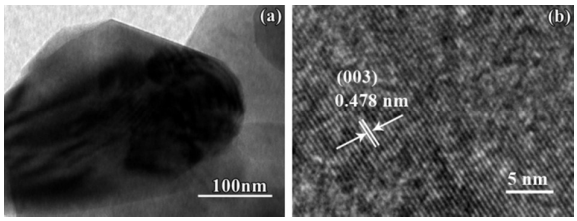

Fig. 4 TEM (a) and HRTEM (b) images of the $LiNi_{0.48}Co_{0.18}Mn_{0.3}Mg_{0.02}Ti_{0.02}O_2$.

investigated by TEM and HR-TEM (Fig. 4). As shown in the micrographs in Fig. 4a and b, the sample has a highly crystalline structure. Fig. 4b shows the clear lattice fringes with an inter-planar distance of about 0.474 nm, which coincides with the d-spacing of the (003) plane of the hexagonal layered structure. Thus, based on the findings of both XRD and SEM, it is clear that the morphology of the pristine material is still well preserved in the doped material, and its layered crystal structure becomes more optimum after introducing Ti and Mg.

3.3 Electrochemical testing

The initial charge/discharge curves at a current density of 0.09 mA cm^{-2} (0.2C) in the voltage range of 2.8-4.3 V at room temperature are shown in Fig. 5. From Fig. 5a, it is evident that the electrode materials show smooth charge and discharge profiles and stable charge/discharge behaviors. It was found that the doping of Mg and Ti leads a slight increase in charge voltage, which should

Journal Name

ARTICLE

Table 3. ICP experiments for the $LiNi_{0.5}Co_{0.2}Mn_{0.3}O_2$ and $LiNi_{0.48}Co_{0.18}Mn_{0.3}Mg_{0.02}Ti_{0.02}O_2$ sample.

Sample	mass ratio (wt.%)					molar ratio (%)				
	Ni	Co	Mn	Mg	Ti	Ni	Co	Mn	Mg	Ti
$LiNi_{0.5}Co_{0.2}Mn_{0.3}O_2$	0.427	0.170	0.243	–	–	0.499	0.198	0.303	–	–
$LiNi_{0.48}Co_{0.18}Mn_{0.3}Mg_{0.02}Ti_{0.02}O_2$	0.410	0.154	0.244	0.007	0.014	0.478	0.179	0.304	0.019	0.020

be attributed to the stronger bonding energy of Mg-Ti-NCM523 than that of the pristine NCM523.[29,30] This is an additional evidence for the incorporation of Mg and Ti in the NMC523 structure.[30, 31] The initial discharge capacity of the $LiNi_{0.48}Co_{0.2}Mn_{0.3}Mg_{0.02}Ti_{0.02}O_2$ (153.1 mAh g^{-1}) is slightly lower than the pristine (159.3 mAh g^{-1}) at 0.2C, with a columbic efficiency enhanced to 83.3% from 82.6% of the pristine sample. This decrease in capacity is mainly caused by doping the electrochemically inactive Mg^{2+} and Ti^{4+} ions. As shown in Fig. 5b, the discharge capacity of $LiNi_{0.5}Co_{0.2}Mn_{0.3}O_2$ abruptly decreases from 159.3 to 132.7 mAh g^{-1} after 50 cycles and the capacity retention is only 83%. On the other hand, the discharge capacity of $LiNi_{0.48}Co_{0.2}Mn_{0.3}Mg_{0.02}Ti_{0.02}O_2$ gradually decreases to 149 mAh g^{-1} and 97% of the capacity is maintained. This enhancement of the initial columbic efficiency and capacity retention should be ascribed to the improved crystal structure, which is in accordance with XRD results.

The rate capability of cathode materials is an important parameter for EVs and renewable energy storage application. Accordingly, the cells were cycled between 2.8-4.3 V, charged at 0.225 mA cm^{-2} (0.5C) and discharged at 0.225 mA cm^{-2} (0.5C), 0.45 mA cm^{-2} (1C), 0.9 mA cm^{-2} (2C), 1.35 mA cm^{-2} (3C) and 2.25 mA cm^{-2} (5C). Firstly, initial cycles of all the cells were selected for clarity (Fig. 6a). The initial discharge capacities for $LiNi_{0.5}Co_{0.2}Mn_{0.3}O_2$ under the different current rates of 0.5C, 1C, 2C, 3C and 5C are 156.9 mAh g^{-1}, 138.9 mAh g^{-1}, 130.7 mAh g^{-1}, 118 mAh g^{-1} and 111.9 mAh g^{-1}, respectively. For $LiNi_{0.48}Co_{0.2}Mn_{0.3}Mg_{0.02}Ti_{0.02}O_2$, the corresponding values are 151.5 mAh g^{-1}, 140.1 mAh g^{-1}, 137.1mAh g^{-1}, 125.2 mAh g^{-1} and 115.3 mAh g^{-1}, respectively. It should be mentioned that the $LiNi_{0.48}Co_{0.2}Mn_{0.3}Mg_{0.02}Ti_{0.02}O_2$ sample, with pristine columbic efficiency of 84%, 75.2%, 70.3%, 63.9%, 60.8%, delivers columbic efficiency increasing to 85.9%, 78.4%, 77.3%, 70.1% and 65.3% at 0.5C, 1C, 2C, 3C and 5C, respectively. Although the initial discharge capacity of $LiNi_{0.48}Co_{0.2}Mn_{0.3}Mg_{0.02}Ti_{0.02}O_2$ at low-C rate (0.5C) rate is slightly lower than the pristine one, its average working potentials obviously decrease more slowly than that of the pristine sample with increasing current density. Hence, the discharge capacities increase at high current density by partial Mg and Ti doping. Further contrasting cycling performances of $LiNi_{0.5}Co_{0.2}Mn_{0.3}O_2$ and $LiNi_{0.48}Co_{0.18}Mn_{0.3}Mg_{0.02}Ti_{0.02}O_2$ samples when cycled from 2.8-4.3 V at different rates, are shown in Fig. 6c and d. It is observed that the discharge capacities for $LiNi_{0.5}Co_{0.2}Mn_{0.3}O_2$ are 129.5 mAh g^{-1}, 118.9 mAh g^{-1}, 106.6 mAh g^{-1}, 96.3 mAh g^{-1} and 87.9 mAh g^{-1} after 100 cycles at 0.5C, 1C, 2C, 3C and 5C, respectively. On the other hand, the $LiNi_{0.48}Co_{0.2}Mn_{0.3}Mg_{0.02}Ti_{0.02}O_2$ sample shows discharge capacities of 142.1 mAh g^{-1}, 129.2 mAh g^{-1}, 127.9 mAh g^{-1}, 121.5 mAh g^{-1} and 108.2 mAh g^{-1} at the 100th cycle, corresponding to the capacity retention of 94%, 96%, 96%, 94%, and 93% of the initial discharge capacity at the same rates. It is noted that $LiNi_{0.48}Co_{0.2}Mn_{0.3}Mg_{0.02}Ti_{0.02}O_2$ delivers better rate performance than the pristine sample at any rate. Even when the rate is as high as 5 C, it delivers an improved reversible capacity of 108.2 mA h g^{-1} with only 7% capacity decrease relative to $LiNi_{0.5}Co_{0.2}Mn_{0.3}O_2$ (23%) after 100 cycles.

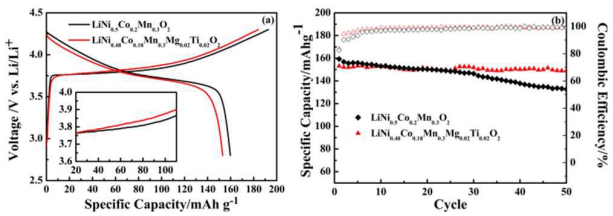

Fig. 5 Initial charge–discharge curves (a) and cycle performances (b) of $LiNi_{0.5}Co_{0.2}Mn_{0.3}O_2$ and $LiNi_{0.48}Co_{0.18}Mn_{0.3}$ $Mg_{0.02}Ti_{0.02}O_2$ samples in the voltage range of 2.8-4.3 V at 0.09 mA cm^{-2} (0.2C) rate.

Fig. 6e shows the rate capability and cycle performances of $LiNi_{0.5}Co_{0.2}Mn_{0.3}O_2$ and $LiNi_{0.48}Co_{0.18}Mn_{0.3}Mg_{0.02}Ti_{0.02}O_2$ samples. The cells were charged at 0.5C and discharged at various current rates (0.5-5C), and each current density was applied for 5 cycles. As

shown in Fig. 6e, $LiNi_{0.48}Co_{0.18}Mn_{0.3}Mg_{0.02}Ti_{0.02}O_2$ can be reversibly cycled at 0.5C, 1C, 2C, 3C and 5C with the discharge capacities of 149.7 mAh g^{-1}, 139.9 mAh g^{-1}, 133.2 mAh g^{-1}, 123 mAh g^{-1} and 116.7 mAh g^{-1}, respectively. More importantly, the discharge capacity of 142.2 mAh g^{-1} could be recovered when the current rate was lowered again to 0.5C. In comparison, the $LiNi_{0.5}Co_{0.2}Mn_{0.3}O_2$ sample delivers a weak performance of rate capacity at high C-rates, although it presents a considerable discharge capacity at low C-rates. The pristine material retains a capacity less than 109.5 mAh g^{-1} at 5C and regains the capacity of only about 135.3 mAh g^{-1} when the current rate returns to 0.5C. Considering the overall results mentioned above, it can be concluded that doping with both Mg and Ti significantly improves the rate and cycle performances of $LiNi_{0.5}Co_{0.2}Mn_{0.3}O_2$.

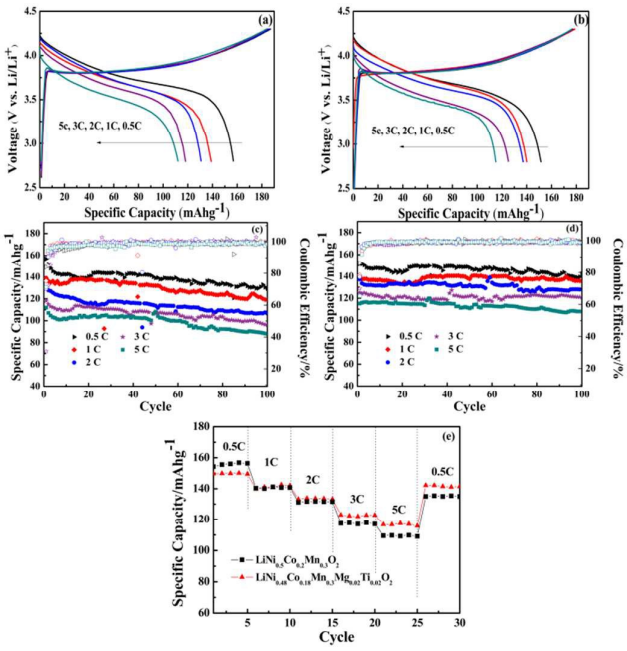

Fig. 6 Initial discharge curves (a, b), cycling performances (c, d) and rate performances (e) of the $LiNi_{0.5}Co_{0.2}Mn_{0.3}O_2$ and $LiNi_{0.48}Co_{0.18}Mn_{0.3}Mg_{0.02}Ti_{0.02}O_2$ samples at different rates (1C=0.45 mA cm^{-2}).

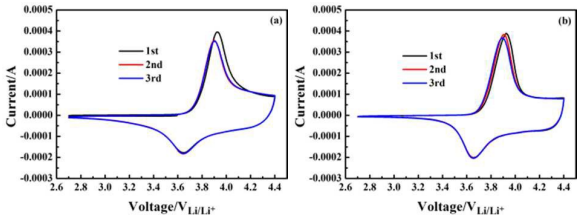

Fig. 7 Cyclic voltammogram (a, b) of $LiNi_{0.5}Co_{0.2}Mn_{0.3}O_2$ and $LiNi_{0.48}Co_{0.18}Mn_{0.3}Mg_{0.02}Ti_{0.02}O_2$ samples at 0.2 mV s^{-1} in the voltage range of 2.7–4.4 V for the first three cycles.

Table 4. The oxidation peak potential ($E_{oxidation}$), reduction peak potential ($E_{reduction}$) and the corresponding difference (ΔE) obtained from CV curves of $LiNi_{0.5}Co_{0.2}Mn_{0.3}O_2$ and $LiNi_{0.48}Co_{0.18}Mn_{0.3}Mg_{0.02}Ti_{0.02}O_2$ for the first three cycles.

Value (V vs. Li/Li^+)	$LiNi_{0.5}Co_{0.2}Mn_{0.3}O_2$			$LiNi_{0.48}Co_{0.18}Mn_{0.3}Mg_{0.02}Ti_{0.02}O_2$		
	1st	2nd	3rd	1st	2nd	3rd
$E_{oxidation}$	3.927	3.903	3.901	3.925	3.895	3.894
$E_{reduction}$	3.649	3.646	3.647	3.657	3.653	3.659
ΔE	0.278	0.257	0.254	0.268	0.242	0.235

Fig. 7 presents the typical CV curves of the pristine and $LiNi_{0.48}Co_{0.18}Mn_{0.3}Mg_{0.02}Ti_{0.02}O_2$ sample between 2.7 V and 4.4 V at a scan rate of 0.2 mV s^{-1}. All the curves exhibit the typical anodic peak of layered $LiNi_{0.5}Co_{0.2}Mn_{0.3}O_2$ at around 3.9 V, which is attributed to oxidation of Ni ions (Ni^{2+}/Ni^{4+}) and Co ions (Co^{3+}/Co^{4+}), accompanied by deintercalation of Li^+ from cathode materials[19]. Furthermore, the relatively broad peaks at around 3.6 V on the discharge curves are ascribed to the reduction of Ni ions (Ni^{4+}/Ni^{2+}) and Co ions (Co^{4+}/Co^{3+}), along with intercalation of Li^+ into cathode materials. Table 4 shows the values for potential difference ΔE ($E_{oxidation}$–$E_{reduction}$) between anodic and cathodic peaks ($E_{oxidation}/E_{reduction}$) of CV curves for the pristine and $LiNi_{0.48}Co_{0.18}Mn_{0.3}Mg_{0.02}Ti_{0.02}O_2$ materials. It is evident that the potential difference ΔE of $LiNi_{0.48}Co_{0.18}Mn_{0.3}Mg_{0.02}Ti_{0.02}O_2$ is less than that of $LiNi_{0.5}Co_{0.2}Mn_{0.3}O_2$, which indicates that the doped material has less polarization. Thus, doping with both Mg and Ti can enhance the reversibility of Li^+ during insertion and extraction and then reduce the capacity fading of NCM523.

To explain the enhanced cycling performance of Mg and Ti co-doped electrodes, EIS was performed. Fig. 8 shows the EIS results of $LiNi_{0.5}Co_{0.2}Mn_{0.3}O_2$ and $LiNi_{0.48}Co_{0.18}Mn_{0.3}Mg_{0.02}Ti_{0.02}O_2$ samples measured after 1st cycle and 50th cycles at 2C. The chemical kinetics are reflected in the measured impedance. The equivalent circuit model of the system to illustrate the impedance data is given in Fig. 8a. As shown in Fig. 8, all EIS plots consist of a depressed semicircle at high-to-medium frequency and an oblique line at low frequency, which can be assigned to interfacial charge transfer resistance (R_{ct}) and Warburg impedance (W), respecti-

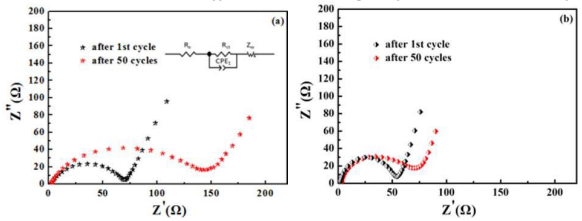

Fig. 8 Nyquist plots (a, b) of $LiNi_{0.5}Co_{0.2}Mn_{0.3}O_2$ and $LiNi_{0.48}Co_{0.18}Mn_{0.3}$ $Mg_{0.02}Ti_{0.02}O$ samples after 1st cycle and 50 cycles at a discharge rate of 2C in the voltage range of 2.8–4.3 V.

vely. The R_{ct} of the pristine sample is 65.49 Ω after the first cycle but increases quickly to 128.9 Ω by the 50th cycle, while the R_{ct} value of $LiNi_{0.48}Co_{0.018}Mn_{0.3}Mg_{0.02}Ti_{0.02}O_2$ increases more slowly. The R_{ct} of the first cycle for the doped sample is 54.78 Ω and 67.78 Ω is obtained after 50 cycles. Thus, even minor Ti and Mg co-doping can facilitate the charge transfer process and decrease the value of R_{ct}, which is advantageous for the rate performance.

Conclusions

$LiNi_{0.48}Co_{0.18}Mn_{0.3}Mg_{0.02}Ti_{0.02}O_2$ has been successfully synthesized via a co-precipitation technique followed by a subsequent high temperature heating step. This material presents typical layer structure and has near-spherical morphology with primary particle size of 400 nm. Moreover, compared with the charge discharge measurements of the $LiNi_{0.5}Co_{0.2}Mn_{0.3}O_2$ sample, $LiNi_{0.48}Co_{0.18}Mn_{0.3}Mg_{0.02}Ti_{0.02}O_2$ has an improved cycling performance and charge/discharge rate but a slightly decreased initial capacity. It delivers the initial discharge capacity of 153.1 mAh g^{-1} at 0.2C over the voltage range of 2.8-4.3 V. After 50 cycles, the discharge capacity of 149 mAh g^{-1} can be obtained. Even at 5C, it exhibits a discharge capacity of 115.3 mAh g^{-1} with 93% capacity retention in 100 cycles. Thus, multi-element doping has great potential for preparing improved layer cathode materials for lithium ion batteries.

Acknowledgements

This work was financially supported by the NSFC (Grant No. 51162006 and Grant No. 51362009), Key science & technology project (ZDXM2015118), International science & technology cooperation program of Hainan (KJHZ2015-02).

Notes and references

1 M. Armand and J.-M. Tarascon, *Nature*, 2008, **451**, 652-657.
2 B. Scrosati, J. Hassoun and Y.-K. Sun, *Energy Environ.Sci.*, 2011, **4**, 3287-3295.
3 J. B. Goodenough and K.-S. Park, *J. Am. Chem. Soc.*, 2013, **135**, 1167-1176.
4 E. Santiago, *Solid State Ionics*, 2003, **158**, 91-102.
5 B. Huang, Y. I. Jang, Y. M. Chiang and D. R. Sadoway, *J. Appl.Electrochem.*, 1998, **28**, 1365-1369.
6 T. Ohzuku and Y. Makimura, *Chem. Lett.*, 2001, 744-745.
7 B. L. Ellis, K. T. Lee and L. F. Nazar, *Chem. Mater.*, 2010, **22**, 691-714.
8 Z. Wang, S. Huang, B. Chen, H. Wu and Y. Zhang, *J. Mater. Chem. A*, 2014, **2**, 19983-19987.
9 X.-H. Liu, L.-Q. Kou, T. Shi, K. Liu and L. Chen, *J. Power Sources*, 2014, **267**, 874-880.
10 S.-K. Jung, H. Gwon, J. Hong, K.-Y. Park, D.-H. Seo, H. Kim, J. Hyun, W. Yang and K. Kang, *Adv. Energy Mater.*, 2014, **4**, 1-7.
11 X. Zhang, W. J. Jiang, A. Mauger, Qilu, F. Gendron and C. M. Julien, *J. Power Sources*, 2010, **195**, 1292 − 1301.
12 L. Cai, Z. Liu, K. An and C. Liang, *J. Electrochem. Soc.*, 2012, **159**, A924-A928.
13 Y. Hinuma, Y. S. Meng, A. Kisuk Kang and G. Ceder, *Chem. Mater.*, 2007, **19**, 1790-1800.
14 A. Boulineau, L. Simonin, J. F. Colin, C. Bourbon and S. Patoux, *Nano Letters*, 2013, **13**, 3857-3863.
15 F. Lin, I. M. Markus, D. Nordlund, T.-C. Weng, M. D. Asta, H. L. Xin and M. M. Doeff, *Nature commun.*, 2014, 5.
16 J. Shu, R. Ma, L. Shao, M. Shui, K. Wu, M. Lao, D. Wang, N. Long and Y. Ren, *J. Power Sources*, 2014, **245**, 7-18.
17 Y.-M. Lee, K.-M. Nam, E.-H. Hwang, Y.-G. Kwon, D.-H. Kang, S.-S. Kim and S.-W. Song, *J. Phys. Chem. C*, 2014, **118**, 10631-10639.
18 P.-Y. Liao, J.-G. Duh and H.-S. Sheu, *J. Power Sources*, 2008, **183**, 766-770.
19 D. Aurbach, O. Srur-Lavi, C. Ghanty, M. Dixit, O. Haik, M. Talianker, Y. Grinblat, N. Leifer, R. Lavi, D. T. Major, G. Goobes, E. Zinigrad, E. M. Erickson, M. Kosa, B. Markovsky, J. Lampert, A. Volkov, J. Y. Shin and A. Garsuch, *J. Electrochem. Soc.*, 2015, **162**, A1014-A1027.
20 N. K. Karan, M. Balasubramanian, D. P. Abraham, M. M. Furczon, D. K. Pradhan, J. J. Saavedra-Arias, R. Thomas and R. S. Katiyar, *J. Power Sources*, 2009, **187**, 586-590.
21 I. M. Markus, F. Lin, K. C. Kam, M. Asta and M. M. Doeff, *J. Phys. Chem. Lett.*, 2014, **5**, 3649-3655.
22 Q. Chen, C. Du, D. Qu, X. Zhang and Z. Tang, *RSC Adv.*, 2015, **5**, 75248-75253.
23 H. Zhu, T. Xie, Z. Chen, L. Li, M. Xu, W. Wang, Y. Lai and J. Li, *Electrochim. Acta*, 2014, **135**, 77-85.
24 S. H. Kang and K. Amine, *J. Power Sources*, 2003, 119-121, 150-155.
25 L. Q. Wang, L. F. Jiao, H. Yuan, J. Guo, M. Zhao, H. X. Li and Y. M. Wang, *J. Power Sources*, 2006, **162**, 1367-1372.
26 T. Ohzuku and A. Ueda, *J. Electrochem. Soc.*, 1994, **141**, 2972-2977.
27 C. Nithya, V. S. Kumari and S. Gopukumar, *ACS Appl. Mater.Interfaces* 2011, **13**, 6125-6132.
28 S. U. Woo, B. C. Park, C. S. Yoon, S. T. Myung, J. Prakash and Y. K. Sun, *J. Electrochem. Soc.*, 2007, **154**, A649-A655.
29 W. M. Haynes, *Crc Press*, 2014.
30 J. Wilcox, S. Patoux and M. Doeff, *J. Electrochem. Soc.*, 2009, **156**, A192-A198.
31 T. E. Conry, A. Mehta, J. Cabana and M. M. Doeff, *Chem. Mater.*, 2012, **24**, 3307-3317.

